because these energies reflect the relative energies of the Mn, Fe, and Rh orbitals. In $[RhFe_3(CO)_{12}C]^-$, where the Rh orbitals are lower in energy than the corresponding Fe orbitals, the cluster orbital having heteroatom character is stabilized and the all-Fe combination is the HOMO. In $[MnFe_3(CO)_{13}C]^-$, where the Mn orbitals are higher in energy than the corresponding Fe orbitals, the cluster orbital having heteroatom character is destabilized and becomes the HOMO. Even though the HOMO's of $[MnFe_3(CO)_{13}C]^-$ and $[RhFe_3(CO)_{12}C]^-$ are different in the hinge region of the clusters, they are very similar in the wingtip region. In this region they both resemble the $5b_2$ orbital of $[Fe_4(CO)_{12}C]^{2-}$, the orbital with which we have associated protonation at the wingtip to ultimately yield a methylidyne cluster. Therefore, just as for $[HFe_4(CO)_{12}C]^-$ the character of the HOMO in both $[RhFe_3(CO)_{12}C]^-$ and $[MnFe_3(CO)_{13}C]^-$ can be associated with the site of proton attack.

Conclusion

In summary, the protonation of carbide clusters with a butterfly array of three irons and a heterometal, Cr, W, Mn, or Rh, occurs at the carbide ligand to produce an agostic C-H--Fe linkage with a wingtip iron atom. By contrast, the first site of protonation in the Fe_4 butterfly carbide cluster, $[Fe_4(CO)_{12}C]^{2-}$, is the Fe-Fe hinge. Fenske-Hall molecular orbital calculations indicate that in the Fe_4 butterfly the HOMO is largely localized on the hinge. This is consistent with protonation at this site. When either a more electronegative metal, Rh, or less electronegative metal, Mn, is introduced into a hinge position in the cluster, the metal-metal-bonding orbitals are perturbed by both the difference in energy between the iron and heterometal orbitals and the lowering of the cluster symmetry. The character and the relative energies of the resulting cluster orbitals depend on the heterometal. In $[RhFe_3(CO)_{12}C]^-$ the orbitals having Rh character are stabilized so that an all-Fe combination is the HOMO. In $[MnFe_3(CO)_{13}C]^-$, on the other hand, an orbital having Mn character is destabilized and becomes the HOMO. In $[RhFe_3(CO)_{12}C]^-$ the high-energy orbitals are further perturbed so that no single metal-metal-bonding orbital is localized across the hinge. Although the characters of the HOMO's are different in the hinge region of the two clusters, in the wingtip region the characters are nearly the same. In both cases, the HOMO extends over the wingtip atoms and correlates with the initial attack of a proton at the wingtip to ultimately form the agostic C-H-Fe bond. The final methylidyne product is not unexpected for $[MnFe_3(CO)_{13}C]^-$ because the hinge M-M bonding orbital is used for bonding with the bridging CO ligand and is thus unavailable for formation of a bridging hydride. For $[RhFe_3(CO)_{12}C]^-$, the calculations suggest that the final methylidyne product is favored over a bridging hydride because of the absence of a very localized hinge bonding orbital.

Acknowledgment. The portion of this research performed at Northwestern University was supported by the NSF Synthetic Inorganic and Organometallic Chemistry Program.

Registry No. $[PPN][CrFe_3(CO)_{13}(CH)]$, 112680-35-0; $[PPN]_2[CrFe_3(CO)_{13}C]$, 88669-42-5; $[PPN][WFe_3(CO)_{13}(CH)]$, 112680-37-2; $[PPN]_2[WFe_3(CO)_{13}C]$, 88657-60-7; $HCrFe_3(CO)_{13}(CH)$, 112680-38-3; $HWFe_3(CO)_{13}(CH)$, 88657-62-9; $[RhFe_3(CO)_{12}C]^-$, 93110-68-0; $[MnFe_3(CO)_{13}C]^-$, 93110-71-5; $[Fe_3(CO)_{10}(CCH_3)]^-$, 87698-66-6; $[Cr_2Fe_3(CO)_{16}C]^{2-}$, 109864-04-2; $[PPN][HWFe_3(CO)_{13}C]$, 112680-40-7; Cr, 7440-47-3; Fe, 7439-89-6; W, 7440-33-7; Rh, 7440-16-6; Mn, 7439-96-5.

Contribution from the Department of Chemistry, Texas A&M University, College Station, Texas 77843

Cluster Synthesis via Aggregation: Synthesis and Solution and Solid-State Characterization of Sulfur-Capped Group 6 Metal Carbonyl Clusters

Donald J. Darensbourg,* David J. Zalewski, Kathryn M. Sanchez, and Terry Delord

Received July 22, 1987

The trinuclear clusters $[PPN]_2[M_3(CO)_{12}S]$ (M = Cr, Mo, W) have been prepared by a stepwise aggregation of $[M(CO)_5]$ fragments about a sulfur atom template, with subsequent loss of three carbonyl ligands concomitant with the formation of three metal-metal bonds. The stepwise assembly process allows for the synthesis of the mixed-metal clusters $[PPN]_2[Cr_2W(CO)_{12}S]$, $[PPN]_2[Mo_2W(CO)_{12}S]$, and $[PPN]_2[CrMoW(CO)_{12}S]$. These compounds have been characterized by infrared and ^{13}C NMR spectroscopies, and X-ray crystal structures of the Cr_3, Mo_3, and Mo_2W clusters have been determined. $[PPN]_2[Cr_3(CO)_{12}S]$: space group $P2_1/c$, a = 25.732 (6) Å, b = 14.255 (5) Å, c = 21.689 (4) Å, β = 96.16 (3)°, V = 7909.8 Å^3, Z = 4. $[PPN]_2[Mo_3(CO)_{12}S]$: space group $P2_1/c$, a = 25.953 (4) Å, b = 14.329 (2) Å, c = 21.830 (5) Å, β = 96.26 (2)°, V = 8069.2 Å^3, Z = 4. $[PPN]_2[Mo_2W(CO)_{12}S]$: space group $P2_1/c$, a = 25.912 (6) Å, b = 14.275 (3) Å, c = 21.871 (3) Å, β = 96.23 (2)°, V = 8042.0 Å^3, Z = 4. The trinuclear clusters can add a fourth $[M(CO)_5]$ unit to produce the tetranuclear derivatives $[PPN]_2[M_4(CO)_{17}S]$. In solution, the carbonyl ligands of both the tri- and tetranuclear clusters are extremely fluxional. Temperatures as low as -110 °C must be achieved to freeze out the various processes.

Introduction

During the last 2 decades organometallic chemists have been actively pursuing the synthesis, chemical reactivity, and spectral/structural properties of discrete molecular transition-metal clusters.[1] Much of this interest originates from the analogy drawn between metal clusters and catalytic surfaces.[2] Polynuclear transition-metal complexes have not yet realized their anticipated potential as homogeneous catalysts;[3] however, metal clusters in and on solid supports (e.g., silica, alumina, magnesia, and zeolites) have provided highly active catalysts or catalyst precursors with surface structures often being similar to the structures of their molecular analogues.[4]

(1) (a) Johnson, B. F. B. *Transition Metal Clusters*; Wiley: New York, 1980. (b) Muetterties, E. L.; Rhodin, T. N.; Band, E.; Brucker, C. F.; Pretzer, W. R. *Chem. Rev.* **1979**, *79*, 91. (c) King, R. B. *Prog. Inorg. Chem.* **1972**, *15*, 287. (d) Canning, N. O. S.; Madix, R. J. *J. Phys. Chem.* **1984**, *88*, 2437. (e) Chini, P., *J. Organomet. Chem.* **1980**, *200*, 379 (f) Vahrenkamp, H., *Struct. Bonding (Berlin)* **1977**, *32*, 1.

(2) (a) Muetterties, E. L. *Bull Soc. Chim. Belg.* **1975**, *84*, 959. (b) Muetterties, E. L. *Bull. Soc. Chim. Belg.* **1976**, *85*, 451. (c) Muetterties, E. L. *Science (Washington, D.C.)* **1971**, *196*, 839.

(3) (a) Laine, R. M. *J. Mol. Catal.* **1982**, *14*, 137. (b) Ugo, R.; Psaro, P. *J. Mol. Catal.* **1983**, *20*, 53. (c) Muetterties, E. L.; Krause, M. J. *Angew. Chem.* **1983**, *95*, 135. (d) Ford, P. C. *Acc. Chem. Res.* **1982**, *14*, 31. (e) Marko, L.; Vizi-Orosz. In *Metal Clusters in Catalysis*; Gates, B. C., Guczi, L. Knözinger, H., Eds.; Elsevier: New York, 1986; p 89.

(4) (a) Psaro, R.; Ugo, R. In *Metal Clusters in Catalysis*; Gates, B. C., Guczi, L., Knözinger, H., Eds.; Elsevier: New York, 1986; p 427. (b) Gates, B. C. In *Heterogeneous Catalysis*; Shapiro, B. L., Ed.; Texas A&M University Press: College Station, TX, 1984; p 1. (c) Gallezot, P. In *Metal Clusters*; Moskovits, M., Ed.; Wiley-Interscience: Toronto, 1986; p 219. (d) Brenner, A. *ibid.*; p 249. (e) Gates, B. C. *ibid.*; p 283.

0020-1669/88/1327-0821$01.50/0

Spectroscopic properties of isolated cluster species are invaluable for the identification of surface species.[5] That is, because the chemical interactions between the transition metal and its ligands in metal clusters can be completely characterized by spectroscopy (infrared, NMR, etc.) and X-ray diffraction analysis, this information on metal–ligand systems can be used in probing catalytic surfaces. An interesting feature associated with metal clusters is that metal atoms in these species can communicate electronic and steric information.[6] Thus by changing the ligand environment of one metal atom in the cluster, it is possible to alter the reactivity at the remaining metal sites. This property offers the possibility to fine tune the reactivity of a metal cluster species. In addition polynuclear transition-metal complexes present the opportunity of multisite activation of a substrate molecule(s).

Two major problems have slowed the development of cluster chemistry. Both of these must be solved before transition-metal cluster compounds can reach their full potential in catalysis. First, systematic routes for the stepwise construction of polynuclear complexes must be developed. These routes must provide opportunities for designing physical constraints into the cluster. Second, the synthesized cluster must be able to withstand the catalytic reaction conditions without undergoing fragmentation processes.

Stone,[7] Osborn,[8] and Vahrenkamp[9] have utilized multidentate ligand systems as templates for the construction of transition-metal clusters. This synthetic methodology provides clusters in which the metal–metal bonds are supported by template ligands. As a result of this, even if the metal–metal bonds are broken during a reaction, the metal atoms are held in place by the template ligand.

In an effort to increase our knowledge of transition-metal clusters, we have exploited the nucleating ability of the sulfur atom and used it as a template for the designed construction of group 6 transition-metal clusters.[10] The sulfur ligand was chosen for the template because of its capability of simultaneously binding to several metal atoms and for its ability to labilize carbonyl ligands.[11] It is this latter feature that induces the formation of the metal–metal bonds.

Experimental Section

All manipulations were performed in a double-manifold Schlenk vacuum line under an atmosphere of dry nitrogen or in an argon-filled drybox. Solvents were dried and deoxygenated by distillation from the appropriate reagent.

Infrared spectra were recorded in 0.10-mm CaF_2 cells on an IBM FT-IR Model 85 spectrometer. ^{13}C NMR spectra were recorded on a Varian XL-200 spectrometer. The samples were prepared by dissolving 100 mg of the compound in 3–5 mL of THF, followed by filtering the solution through a silica gel column into a 10-mm NMR tube. A 0.10-mL sample of acetone-d_6 or benzene-d_6 was added for the deuterium lock. The spectra were referenced relative to Me_4Si by employing the solvent peaks.

Elemental analysis were performed by Galbraith Laboratories, Knoxville, TN.

Compound Preparations. **$[Cr_3(CO)_{12}S][PPN]_2$.** A 0.147-g sample of NaSH (2.63 mmol) and 1.27 g of [PPN]Cl (2.21 mmol) were placed in a 50-mL Schlenk flask and stirred with 10 mL of EtOH for 2 h. The solvent was then removed in vacuo. A condenser was attached to the flask, and 0.504 g of $Cr(CO)_6$ (2.29 mmol) was added along with 10 mL of THF. Refluxing the mixture for 1 h resulted in the formation of the yellow $[Cr(CO)_5SH]PPN$. A stainless-steel cannula was used to transfer the solution into a 100-mL Schlenk flask. Then, 1.13 g $Cr(CO)_6$ (5.16 mmol) was photolyzed in 60 mL of THF to convert it into $Cr(CO)_5THF$. Half of this solution was added to the flask containing the $[Cr(CO)_5SH]PPN$. After the addition, the solution turned to the orange color of $[Cr_2(CO)_{10}SH]PPN$. A 0.106-g sample of NaH (60% dispersion in mineral oil, 2.65 mmol) was then added, turning the orange solution into the dark green color of $[Cr_2(CO)_{10}S]^{2-}$. Addition of the remaining $Cr(CO)_5THF$ solution changed the color to brown. The solution was stirred for 2 h, followed by the addition of 1.27 g of [PPN]Cl (2.22 mmol) in 7 mL of EtOH. After the solution was stirred overnight, the solvent was removed in vacuo. The resulting residue was dissolved in acetone and precipitated with ether to give 1.20 g of red crystals of $[Cr_3(CO)_{12}S][PPN]_2 \cdot CH_3C(O)CH_3$ (32.8% yield). ^{13}C NMR (ppm): 254.0, 236.1, 229.7. IR (cm^{-1} in THF): 2008 (vw), 1946 (vs), 1898 (s), 1847 (m), 1787 (w, br), 1718 (w). Anal. Calcd: C, 62.97; H, 4.01; N, 1.69; P, 7.47; S, 1.93. Found: C, 63.10; H, 4.18; N, 1.50; P, 7.55; S, 2.03.

$[Mo_3(CO)_{12}S][PPN]_2$. A 0.0712-g sample of NaSH (1.25 mmol) and 0.640 g of [PPN]Cl (1.11 mmol) were stirred in 10 mL of EtOH for 2 h and then pumped to dryness. Then 0.587 of $Mo(CO)_6$ (2.22 mmol) was added along with 10 mL of THF. Stirring the mixture for 1 day gave an orange solution of $[Mo_2(CO)_{10}SH][PPN]$. A cannula was used to transfer the solution to a 100-mL Schlenk flask containing NaH (~2 mmol). A 0.310-g sample of $Mo(CO)_6$ (1.2 mmol), converted to $Mo(CO)_5THF$ by photolysis, was then added. After 1 h, 0.638 g of [PPN]Cl (1.11 mmol) in 5 mL of EtOH was added. After the solution was stirred for 1 h, the solvent was removed in vacuo. The residue was then dissolved in acetone, and orange crystals of $[Mo_3(CO)_{12}S][PPN]_2 \cdot CH_3C(O)CH_3$ precipitated upon the addition of ether. The cluster was recrystallized twice to give 1.25 g of product, 62.6% yield. ^{13}C NMR (ppm): 239.7, 221.7, 215.8. IR (cm^{-1} in THF): 2057 (vw), 2017 (vw), 1968 (s), 1941 (m), 1906 (vs), 1897 (sh), 1845 (7), 1808 (w, br), 1716 (w). Anal. Calcd: C, 58.34; H, 3.71; N, 1.56; P, 6.92; S, 1.79. Found: C, 58.44; H, 3.92; N, 1.51; P, 6.70; S, 1.73.

$[W_3(CO)_{12}S][PPN]_2$. A 0.0478-g sample of NaSH (0.85 mmol) and 0.461 g of [PPN]Cl (0.80 mmol) were stirred for 2 h in 10 mL of EtOH and the mixture was then pumped to dryness. A 0.570-g sample of $W(CO)_6$ (1.62 mmol) and 10 mL of THF were added. Stirring the mixture overnight formed the yellow $[W(CO)_5SH]PPN$. Refluxing the solution for 1.5 h led to the formation of $[W_2(CO)_{10}SH]PPN$. After cooling, the solution was transferred via cannula to a flask containing NaH. This caused the organge solution to turn into the dark green color of $[W_2(CO)_{10}S]^{2-}$. Then 0.296 g of $W(CO)_6$ (0.84 mmol) converted to $W(CO)_5THF$ by photolysis was added. The resulting green solution turned brown upon photolysis for an hour. The brown solution was transferred to a flask containing 0.465 g of [PPN]Cl in 5 mL of EtOH and stirred for 1 h, followed by pumping to dryness. The residue was dissolved in acetone, and the orange product precipitated upon the addition of ether. The product was recrystallized three times to give 0.800 g of $[W_3(CO)_{12}S][PPN]_2 \cdot CH_3C(O)CH_3$ (48.5% yield). ^{13}C NMR (ppm): 224.7 (J = 26.3 Hz), 214.0 (J = 76.3 Hz), 204.5 (J = 81.3 Hz). IR (cm^{-1} in THF): 2039 (vw), 2016 (vw), 1965 (s), 1905 (s), 1898 (sh), 1845 (m), 1798 (w, br), 1716 (w). Anal. Calcd: C, 50.56; H, 3.23; P, 6.00. Found: C, 50.58; H, 3.24; P, 6.03.

$[Cr_2W(CO)_{12}S][PPN]_2$. A 0.0955-g sample of NaSH (1.79 mmol) and 0.869 of [PPN]Cl (1.51 mmol) were stirred in 10 mL of EtOH for 2 h, and the mixture was then pumped to dryness. A 0.482-g sample of $W(CO)_6$ (1.37 mmol) was added along with 10 mL of THF. After the solution was refluxed for 1 h, it was slowly cooled to room temperature, filtered, and pumped down to an oil. Then 15 mL of hexane was added to the oil, and the mixture was stirred in an ice bath for several hours to give a yellow solid $[W(CO)_5SH]PPN$ (1.088 g, 89.1% yield). A 0.585-g sample of $Cr(CO)_6$ (2.66 mmol) was photolyzed in 60 mL of THF to form $Cr(CO)_5THF$. Half of this solution was added to a flask containing $[W(CO)_5SH]PPN$ compound to form $[WCr(CO)_{10}SH]PPN$. This mixed-metal dimer was then converted to the dianion by the addition of NaH. The remaining $Cr(CO)_5THF$ solution was added along with 0.700 g of [PPN]Cl (1.22 mmol) in 5 mL of EtOH. The solution was stirred for 1 h and then pumped to dryness. The product was recrystallized three times from acetone/ether to give 0.978 g of $[Cr_2W(CO)_{12}S][PPN]_2 \cdot CH_3C(O)CH_3$ (44.8% yield). Anal. Calcd: C, 58.33; H, 3.71; S, 1.79; P, 6.92; Cr, 5.70; W, 10.20. Found: C, 56.25; H, 3.85; S, 1.54; P, 6 81; Cr, 3.90; W, 14.64.

$[Mo_2W(CO)_{12}S][PPN]_2$. A solution of 0.098 g of NaSH (1.7 mmol), 0.931 g of [PPN]Cl (1.06 mmol), and 10 mL of EtOH contained in a

(5) See for example the many excellent chapters in: *Metal Clusters in Catalysis*; Gates, B. C., Guczi, L., Knözinger, H., Eds.; Elsevier: New York, 1986.
(6) (a) Karel, K. J.; Norton, J. R. *J. Am. Chem. Soc.* **1974**, *96*, 6812. (b) Sonnenberger, D.; Atwood, J. D. *J. Am. Chem. Soc.* **1982**, *104*, 2114. (c) Atwood, J. D.; Wovkulich, M. J.; Sonnenberger, D. *Acc. Chem. Res.* **1983**, *16*, 350. (d) Darensbourg, D. J.; Zalewski, D. J. *Organometallics* **1985**, *4*, 92. (e) Darensbourg, D. J.; Zalewski, D. J.; Delord, T. *Organometallics* **1984**, *3*, 1210.
(7) (a) Stone, F. G. A. *Angew. Chem., Int. Ed. Eng.* **1984**, *23*, 89. (b) Stone, F. G. A.; et al. *J. Chem. Soc., Chem. Commun.* **1980**, 1057.
(8) (a) Osborn, J. A., Stanley, G. G. *Angew. Chem., Int. Ed. Eng.* **1980**, *19*, 1025. (b) Bahsoun, A. A.; Osborn, J. A.; Voelken, C.; Bonnet, J. J.; Lavigne, G. *Organometallics* **1982**, *1*, 1114.
(9) (a) Vahrenkamp, H. *Adv. Organomet. Chem.* **1983**, *22*, 169. (b) Vahrenkamp, H.; Fischer, K.; Muller, M. *Angew. Chem., Int. Ed. Engl.* **1984**, *23*, 1114.
(10) Darensbourg, D. J.; Zalewski, D. J. *Organometallics* **1984**, *3*, 1598.
(11) Darensbourg, D. J.; Rokicki, A.; Kudaroski, R. *Organometallics* **1982**, *1*, 1161.

Table I. Crystal and Data Collection Parameters for the $[M_3(CO)_{12}S][PPN]_2$ Clusters

formula	$Cr_3SP_4O_{13}N_2C_{87}H_{66}$	$Mo_3SP_4O_{13}N_2C_{87}H_{66}$	$WMo_2SP_4O_{13}N_2C_{87}H_{66}$
mol wt	1659.4	1791.3	1879.2
space group	$P2_1/c$	$P2_1/c$	$P2_1/c$
cell dimens			
a, Å	25.732 (6)	25.953 (4)	25.912 (6)
b, Å	14.255 (5)	14.329 (2)	14.275 (3)
c, Å	21.689 (4)	21.830 (5)	21.871 (3)
β, deg	96.16 (3)	96.26 (2)	96.23 (2)
V, Å^3	7909.8	8069.2	8042.0
Z	4	4	4
D_c(calcd), g cm^{-3}	1.39	1.47	1.55
μ, cm^{-1}	1.26	5.33	5.64
variables refined	327	367	369
no. of obsd reflcns ($I > 3\sigma(I)$)	4030	9341	9109
no. of data used	1700	6216	5916
R	0.097	0.064	0.059
R_w	0.0869	0.069	0.063
largest shift, final cycle	0.01σ	0.03σ	0.05σ
largest residue, e/Å^3	0.54	0.79	0.74

Schlenk flask was stirred for 3 h. The solvent was removed in vacuo. A 0.868-g sample of $Mo(CO)_6$ (3.3 mmol) and 10 mL of THF were added. The mixture was allowed to stir overnight, and 10 mL of diethyl ether was then added to precipitate the small amount of $[Mo(CO)_5SH]PPN$ that formed, leaving $[Mo_2(CO)_{10}SH]PPN$ in solution. The solution was transferred with the use of a stainless-steel cannula to a 50-mL Schlenk flask. The solvent was removed in vacuo. The residue was washed with several portions of hexane to remove any unreacted $Mo(CO)_6$, and 15 mL of THF was added to dissolve the $[Mo_2(CO)_{10}SH]PPN$. This solution was transferred to a flask containing NaH. A 0.555-g sample of $W(CO)_6$ (1.58 mmol) converted to $W(CO)_5THF$ by photolysis was then added. After 1 h, 0.925 g of [PPN]Cl in 10 mL of EtOH was added. After the solution was stirred for 1 h, the solvent was removed, and the product was recrystallized from acetone upon the addition of diethyl ether. A total of 1.088 g of orange crystals was recovered (35.5% yield). IR (cm^{-1} in THF): 2039 (vw), 2019 (vw), 1970 (s), 1908 (s), 1900 (sh), 1847 (m), 1803 (br). Anal. Calcd: Mo, 11.65; W, 7.38; C, 56.28. Found: Mo, 11.24; W, 6.98; C, 56.93.

$[CrMoW(CO)_{12}S][PPN]_2$. A Schlenk flask containing 0.04 g of NaSH (0.7 mmol), 0.365 g of [PPN]Cl (0.627 mmol), and 10 mL of EtOH was stirred for 3 h. The solvent was then removed in vacuo. A 0.165-g sample of $W(CO)_6$ (0.469 mmol) and 10 mL of THF were then added. The solution was refluxed for 1 h to form the yellow-orange $[W(CO)_5SH][PPN]$. After the solution was cooled in a dry ice/acetone slush for 1.5 h, it was filtered through a medium porosity frit. A 0.105-g sample of $Cr(CO)_6$ (0.478 mmol) was when photolyzed in 50 mL of THF for 75 min and added to the above solution. The resulting red solution was transferred to a flask containing 0.1 g of NaH, changing the color of the solution to dark green. Then 0.127 g of $Mo(CO)_6$ (0.482 mmol) was photolyzed in 50 mL of THF for 75 min and added to the above mixture. A 0.296-g sample of [PPN]Cl (0.516 mmol) in 5 mL of EtOH was then added. After the solution was stirred for 1 h, the solvent was removed, and the product was recrystallized from acetone upon the addition of diethyl ether. A total of 0.109 g of orange crystals was recovered (12.6% yield). IR (cm^{-1} in THF): 2040 (vw), 1967 (s), 1907 (s), 1900 (sh), 1848 (m), 1796 (br).

X-ray Experimental Data. X-ray quality crystals were grown from acetone solutions upon the addition of diethyl ether. Crystals used for data collection were sealed in epoxy inside a glass capillary tube in order to prevent atmospheric contact. Intensity data were collected on an Enraf-Nonius CAD4 computer automated diffractometer by using Mo Kα radiation (λ = 0.71073 Å) at ambient temperature. Precise lattice constants determined from 25 well-centered reflections gave the values listed in Table I. Unique data were collected ($h, k \geq 0, \pm l$) in the range $0° < \theta < 22°$. Data were corrected for Lorentz and polarization effects but not absorption (μ = 15.7 cm^{-1}).

The locations of the three Mo atoms in $[Mo_3(CO)_{12}S][PPN]_2$ were determined from application of the direct-methods portion of the Enraf-Nonius SDP system of programs.[12] Due to the large number of parameters associated with the $[PPN]^+$ cation, refinement was carried out by using the program SHELX 76 for rigid-body calculations.[13] All phenyl rings were refined as rigid bodies by converting approximate coordinates for the six carbon atoms of the ring to a regular hexagon with the C–C bond distance fixed at 1.395 Å. All hydrogen atoms were included in idealized, calculated positions without refinement. All nonphenyl, non-hydrogen atoms of the structure were allowed to refine anisotropically. The structure was refined by using full-matrix weighted least squares where the function minimized was $\sum w(|F_o| - |F_c|)^2$ and the weight w is defined as $4F_o^2/\sigma^2(F_o^2)$.

The isomorphorus character of this cluster system allowed us to use the Mo_3 data to solve the structure of the Cr_3 and WMo_2 clusters. Tables II–IV list the atomic positional and isotropic temperature factors for these three compounds. Tables V and VI list the selected bond distances and bond angles for the clusters.

Table II. Selected Atomic Positional Parameters ($\times 10^4$) and Isotropic Temperature Factors (Å$^2 \times 10^3$) for $[Cr_3(CO)_{12}S][PPN]_2$

atom	x	y	z	U
Cr_1	2553 (3)	1697 (5)	9197 (3)	55 (4)[a]
Cr_2	1510 (3)	1429 (6)	9527 (3)	62 (4)[a]
Cr_3	2243 (3)	2423 (5)	10321 (3)	52 (3)[a]
S	1923 (4)	2826 (8)	9328 (5	57 (6)[a]
O_{1A}	2286 (13)	1994 (23)	7818 (14)	107 (18)[a]
O_{1B}	3457 (11)	2931 (22)	9064 (14)	100 (18)[a]
O_{1C}	3114 (14)	−104 (29)	8869 (16)	114 (20)[a]
O_{1D}	3241 (11)	990 (22)	10343 (15)	94 (17)[a]
O_{2A}	626 (11)	2676 (26)	9901 (14)	108 (18)[a]
O_{2B}	894 (13)	−194 (25)	9917 (14)	102 (19)[a]
O_{2C}	1005 (12)	1548 (24)	8238 (14)	98 (17)[a]
O_{2D}	2051 (14)	−421 (28)	9361 (17)	121 (20)[a]
O_{3A}	2834 (11)	4240 (24)	10278 (15)	94 (18)[a]
O_{3B}	1487 (11)	3469 (22)	10995 (14)	96 (16)[a]
O_{3C}	2861 (11)	1927 (22)	11524 (13)	95 (16)[a]
O_{3D}	1857 (11)	618 (20)	10871 (14)	81 (15)[a]
C_{1A}	2379 (18)	1908 (34)	8320 (21)	61 (17)
C_{1B}	3078 (19)	2433 (37)	9075 (20)	70 (16)
C_{1C}	2906 (23)	620 (43)	8985 (27)	104 (26)
C_{1D}	2911 (20)	1335 (38)	10013 (22)	77 (19)
C_{2A}	945 (18)	2226 (32)	9790 (20)	59 (18)
C_{2B}	1133 (22)	465 (43)	9735 (24)	94 (23)
C_{2C}	1213 (21)	1428 (40)	8714 (26)	102 (24)
C_{2D}	1929 (20)	345 (37)	9380 (24)	62 (19)
C_{3A}	2641 (15)	3517 (30)	10304 (17)	27 (14)
C_{3B}	1828 (18)	3064 (32)	10752 (20)	60 (16)
C_{3C}	2626 (18)	2141 (34)	11059 (21)	68 (18)
C_{3D}	1940 (15)	1246 (31)	10519 (17)	32 (12)

[a] Equivalent isotropic temperature factor.

Results and Discussion

The SH^- moiety reacts readily with group 6 hexacarbonyls to give the well known pentacarbonylmetal thiolate complexes, $M(CO)_5SH^-$.[14] These species can react with a second pentacarbonyl metal fragment to form the bis(pentacarbonylmetal)-thiolate complexes $[M_2(CO)_{10}SH]^-$. The dinuclear species contains two pentacarbonylmetal moieties held together by a bridging thiolate ligand. No metal–metal bonding is present in this com-

(12) Sheldrick, G. "SHELX 76, Program for Crystal Structure Determination", 1976.
(13) "Structure Determination Programs" (SDP); Enraf-Nonius: Delft, Holland, 1975 (revised 1981).
(14) Gingerich, R. G. W.; Angelici, R. J. *J. Am. Chem. Soc.* **1979**, *101*, 5604.

Table III. Selected Atomic Positional Parameters (×10⁴) and Isotropic Temperature Factors (Å² × 10³) for $[Mo_3(CO)_{12}S][PPN]_2$

atom	x	y	z	U^a
Mo_1	2565 (1)	1740 (1)	9168 (1)	50 (1)
Mo_2	1471 (1)	1454 (1)	9525 (1)	48 (1)
Mo_3	2250 (1)	2496 (1)	10371 (1)	46 (1)
S_1	1905 (1)	2942 (2)	9320 (1)	51 (1)
O_{1A}	2248 (4)	2088 (7)	7744 (4)	101 (5)
O_{1B}	3512 (4)	3005 (8)	9039 (5)	107 (5)
O_{1C}	3132 (4)	−79 (7)	8845 (5)	101 (5)
O_{1D}	3246 (3)	967 (7)	10342 (4)	84 (4)
O_{2A}	565 (4)	2705 (8)	9930 (5)	104 (5)
O_{2B}	837 (4)	−255 (7)	9898 (4)	104 (5)
O_{2C}	956 (4)	1533 (9)	8164 (4)	117 (6)
O_{2D}	2049 (4)	−447 (7)	9349 (5)	96 (5)
O_{3A}	2870 (4)	4398 (7)	10371 (5)	96 (5)
O_{3B}	1459 (4)	3507 (7)	11093 (5)	104 (5)
O_{3C}	2908 (4)	1957 (7)	11581 (4)	90 (4)
O_{3D}	1872 (3)	594 (6)	10903 (4)	71 (4)
C_{1A}	2337 (5)	1941 (9)	8253 (6)	62 (5)
C_{1B}	3152 (5)	2536 (10)	9090 (6)	69 (5)
C_{1C}	2928 (5)	604 (10)	8959 (7)	77 (6)
C_{1D}	2944 (4)	1360 (9)	10000 (5)	57 (5)
C_{2A}	900 (5)	2264 (10)	9782 (6)	69 (5)
C_{2B}	1067 (5)	396 (10)	9761 (5)	68 (5)
C_{2C}	1137 (5)	1458 (10)	8671 (7)	76 (6)
C_{2D}	1929 (5)	330 (10)	9370 (6)	65 (5)
C_{3A}	2658 (5)	3699 (9)	10357 (5)	57 (5)
C_{3B}	1763 (5)	3144 (8)	10823 (6)	62 (5)
C_{3C}	2664 (5)	2163 (9)	11131 (6)	61 (5)
C_{3D}	1927 (4)	1224 (8)	10596 (5)	51 (4)

[a] Equivalent isotropic temperature factor.

Table IV. Selected Atomic Positional Parameters (×10⁴) and Isotropic Temperature Factors (Å² × 10³) for $[Mo_2W(CO)_{12}S][PPN]_2$

atom	x	y	z	U^a
MO_1	2566 (1)	1744 (1)	9172 (1)	52 (1)
Mo_2	1471 (1)	1452 (1)	9522 (1)	51 (1)
Mo_3	2246 (1)	2496 (1)	10373 (1)	49 (1)
W_1	2566 (1)	1744 (1)	9172 (1)	52 (1)
W_2	1471 (1)	1452 (1)	9522 (1)	51 (1)
W_3	2246 (1)	2496 (1)	10373 (1)	49 (1)
S	1904 (1)	2943 (3)	9320 (2)	62 (1)
O_{1A}	2249 (5)	2075 (8)	7744 (5)	116 (6)
O_{1B}	3508 (4)	3020 (9)	9038 (6)	119 (6)
O_{1C}	3123 (5)	−85 (9)	8842 (6)	119 (6)
O_{1D}	3240 (4)	974 (8)	10342 (5)	100 (5)
O_{2A}	553 (5)	2716 (10)	9934 (6)	131 (6)
O_{2B}	842 (5)	−245 (9)	9902 (5)	128 (6)
O_{2C}	956 (4)	1540 (11)	8158 (5)	127 (6)
O_{2D}	2056 (5)	−461 (8)	9356 (6)	119 (6)
O_{3A}	2868 (4)	4381 (8)	10375 (5)	109 (5)
O_{3B}	1454 (5)	3501 (8)	11091 (6)	122 (6)
O_{3C}	2900 (4)	1967 (7)	11580 (5)	101 (5)
O_{3D}	1872 (4)	583 (7)	10902 (4)	86 (4)
C_{1A}	2351 (6)	1912 (11)	8275 (8)	80 (7)
C_{1B}	3143 (6)	2525 (13)	9082 (7)	88 (7)
C_{1C}	2913 (6)	609 (12)	8946 (7)	87 (7)
C_{1D}	2931 (5)	1364 (10)	9992 (7)	67 (6)
C_{2A}	897 (7)	2279 (12)	9774 (7)	87 (7)
C_{2B}	1077 (6)	390 (12)	9751 (6)	80 (7)
C_{2C}	1145 (6)	1457 (11)	8678 (8)	86 (7)
C_{2D}	1931 (6)	330 (12)	9365 (7)	79 (7)
C_{3A}	2646 (5)	3668 (11)	10369 (7)	71 (6)
C_{3B}	1771 (6)	3133 (10)	10825 (7)	74 (6)
C_{3C}	2652 (6)	2161 (10)	11113 (7)	74 (6)
C_{3D}	1929 (5)	1232 (10)	10598 (6)	64 (6)

[a] Equivalent isotropic temperature factor.

pound. Before a third pentacarbonyl fragment can be added to the sulfur atom, the nucleophilicity of sulfur must be enhanced. This can be accomplished by deprotonating $[M_2(CO)_{10}SH]^-$ with NaH.[15] This reaction liberates H_2 and forms the dark green dianionic derivative $[M_2(CO)_{10}S]^{2-}$. The addition of $M(CO)_5$ to the dimeric dianion proceeds smoothly to give the trinuclear pentacarbonyl complex $[(M(CO)_5)_3S]^{2-}$. This complex is unstable, slowly losing three carbon monoxide groups with the simultaneous formation of three metal–metal bonds to form the sulfur-capped cluster $[M_3(CO)_{12}S]^{2-}$ (eq 1).

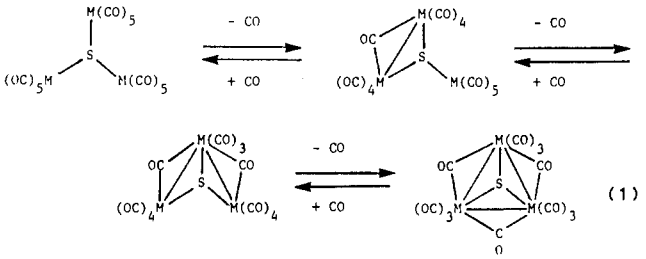

(1)

Loss of the three carbonyl groups is believed to occur stepwise and reversibly. When $[M_3(CO)_{12}S]^{2-}$ is reacted with CO at 0 °C a color change (red–brown–green–yellow) is observed. Along with this color change all of the infrared bands assigned to the bridging carbonyl groups slowly disappear. The yellow solution contains an IR band pattern consistent with a C_{4v} $M(CO)_5$ arrangement and is assigned to a pentacarbonyl species $[M(CO)_5]_3S[PPN]_2$. Superimposed on this pattern is an IR band assigned to $M(CO)_6$ resulting from decomposition. Purging the CO from the system leads to formation of the original cluster. Attempts to isolate either of the intermediates have thus far been unsuccessful.

Since these clusters are synthesized in a stepwise fashion, it is possible to incorporate different metal atoms into the same discrete metal cluster. This provides the opportunity to construct a discrete molecular cluster containing each member of the group 6 metal triad, i.e., $[CrMoW(CO)_{12}S][PPN]_2$. This unique cluster possesses a chiral M_3S core about which 12 carbonyl ligands orient themselves. The chirality imposed by this metal core could lead to very selective reactivity. Being able to selectively substitute metal atoms into a cluster provides one with the opportunity to evaluate the subtle electronic influences imposed by different metal atoms.

The trinuclear clusters can react with a fourth pentacarbonyl fragment to give the tetranuclear derivative $[M_4(CO)_{17}S][PPN]_2$.

Table V. Selected Bond Distances (Å) for the $[M_3(CO)_{12}S][PPN]_2$ Clusters

	Mo_3	Cr_3	Mo_2W
M_2-M_1	3.054 (2)	2.875 (14)	3.047 (2)
M_3-M_1	3.040 (2)	2.840 (14)	3.036 (2)
M_2-M_3	2.987 (2)	2.797 (16)	2.984 (2)
$S-M_1$	2.474 (2)	2.324 (20)	2.469 (5)
$S-M_2$	2.472 (4)	2.319 (20)	2.468 (5)
$S-M_3$	2.459 (4)	2.294 (20)	2.460 (5)
M_1-C_{1A}	2.047 (19)	1.930 (70)	1.994 (23)
M_1-C_{1B}	1.925 (20)	1.753 (78)	1.891 (24)
M_1-C_{1C}	1.958 (20)	1.867 (91)	1.942 (23)
M_1-C_{1D}	2.045 (17)	1.973 (75)	2.009 (19)
M_2-C_{2A}	2.009 (20)	1.977 (71)	2.023 (24)
M_2-C_{2B}	1.942 (20)	1.769 (92)	1.926 (23)
M_2-C_{2C}	1.970 (23)	1.846 (83)	1.946 (24)
M_2-C_{2D}	2.051 (21)	1.930 (79)	2.047 (23)
M_3-C_{3A}	2.021 (20)	1.868 (65)	1.968 (21)
M_3-C_{3B}	1.925 (18)	1.750 (72)	1.894 (20)
M_3-C_{3C}	1.937 (18)	1.833 (70)	1.892 (20)
M_3-C_{3D}	2.084 (17)	1.918 (66)	2.063 (20)
$C_{1A}-O_{1A}$	1.131 (18)	1.097 (63)	1.186 (21)
$C_{1B}-O_{1B}$	1.163 (20)	1.210 (70)	1.192 (23)
$C_{1C}-O_{1C}$	1.150 (20)	1.201 (83)	1.165 (22)
$C_{1D}-O_{1D}$	1.167 (17)	1.161 (71)	1.185 (19)
$C_{2A}-O_{2A}$	1.147 (19)	1.088 (65)	1.171 (22)
$C_{2B}-O_{2B}$	1.163 (19)	1.211 (80)	1.158 (21)
$C_{2C}-O_{2C}$	1.162 (21)	1.123 (75)	1.193 (23)
$C_{2D}-O_{2D}$	1.155 (19)	1.139 (72)	1.175 (21)
$C_{3A}-O_{3A}$	1.140 (18)	1.149 (62)	1.169 (20)
$C_{3B}-O_{3B}$	1.159 (18)	1.217 (64)	1.180 (20)
$C_{3C}-O_{3C}$	1.151 (18)	1.160 (66)	1.179 (20)
$C_{3D}-O_{3D}$	1.143 (17)	1.210 (59)	1.159 (18)

(15) Angelici, R. J.; Gingerich, R. G. W. *Organometallics* **1983**, *2*, 89.

Table VI. Selected Bond Angles (deg) for the $[M_3(CO)_{12}S][PPN]_2$ Clusters

	Mo_3	Cr_3	Mo_2W
M_2-M_1-M_3	58.7 (0)	58.6 (4)	58.8 (0)
M_1-M_2-M_3	60.4 (0)	60.1 (4)	60.4 (0)
M_1-M_3-M_2	60.9 (0)	61.3 (4)	60.8 (0)
S-M_1-M_2	51.8 (1)	51.7 (5)	51.9 (1)
S-M_1-M_3	51.7 (1)	51.6 (5)	51.9 (1)
S-M_2-M_1	51.9 (1)	51.8 (5)	51.9 (1)
S-M_2-M_3	52.5 (1)	52.3 (5)	52.6 (1)
S-M_3-M_1	52.2 (1)	52.5 (5)	52.1 (1)
S-M_3-M_2	52.9 (1)	53.1 (5)	52.8 (1)
C_{1A}-M_1-M_2	95.3 (5)	98.2 (21)	95.5 (6)
C_{1A}-M_1-M_3	136.2 (5)	137.1 (22)	137.4 (6)
C_{1A}-M_1-S	84.5 (5)	85.5 (22)	85.6 (6)
C_{1B}-M_1-M_2	150.4 (6)	150.6 (24)	151.0 (6)
C_{1B}-M_1-M_3	99.1 (5)	101.7 (22)	100.0 (6)
C_{1B}-M_1-S	99.6 (6)	99.3 (24)	100.0 (6)
C_{1B}-M_1-C_{1A}	88.6 (7)	81.9 (29)	88.1 (9)
C_{1C}-M_1-M_2	115.7 (6)	116.4 (27)	114.8 (6)
C_{1C}-M_1-M_3	132.9 (6)	134.4 (28)	133.8 (6)
C_{1C}-M_1-S	165.1 (6)	164.7 (29)	163.5 (6)
C_{1C}-M_1-C_{1A}	89.0 (8)	87.3 (33)	86.4 (8)
C_{1C}-M_1-C_{1B}	93.6 (8)	93.0 (35)	94.2 (9)
C_{1D}-M_1-M_2	96.2 (5)	95.7 (22)	95.7 (5)
C_{1D}-M_1-M_3	58.1 (5)	58.2 (23)	57.9 (5)
C_{1D}-M_1-S	109.7 (5)	109.6 (23)	109.6 (5)
C_{1D}-M_1-C_{1A}	165.4 (7)	163.9 (31)	164 (8)
C_{1D}-M_1-C_{1B}	85.9 (7)	89.9 (32)	87.2 (8)
C_{1D}-M_1-C_{1C}	78.0 (8)	79.2 (36)	79.4 (8)
C_{2A}-M_2-M_1	136.9 (5)	136.9 (20)	136.2 (6)
C_{2A}-M_2-M_3	90.5 (5)	90.0 (20)	90.2 (6)
C_{2A}-M_2-S	85.4 (5)	85.7 (20)	84.7 (6)
C_{2B}-M_2-M_1	135.7 (6)	136.0 (27)	135.1 (6)
C_{2B}-M_2-M_3	124.9 (5)	126.1 (27)	124.8 (6)
C_{2B}-M_2-S	171.4 (5)	171.7 (27)	172.0 (6)
C_{2B}-M_2-C_{2A}	86.5 (8)	86.1 (33)	87.8 (8)
C_{2C}-M_2-M_1	94.7 (5)	93.7 (25)	94.7 (5)
C_{2C}-M_2-M_3	141.6 (5)	140.5 (27)	141.6 (6)
C_{2C}-M_2-S	89.3 (6)	88.6 (27)	89.2 (6)
C_{2C}-M_2-C_{2A}	90.2 (7)	91.9 (33)	90.0 (8)
C_{2C}-M_2-C_{2B}	93.5 (7)	93.4 (37)	93.5 (8)
C_{2D}-M_2-M_1	59.3 (5)	60.8 (23)	59.4 (6)
C_{2D}-M_2-M_3	97.3 (5)	98.9 (24)	97.5 (6)
C_{2D}-M_2-S	111.1 (5)	112.5 (23)	111.1 (6)
C_{2D}-M_2-C_{2A}	163.2 (7)	161.6 (30)	164.0 (8)
C_{2D}-M_2-C_{2B}	76.9 (7)	75.6 (33)	76.3 (8)
C_{2D}-M_2-C_{2C}	92.8 (7)	91.3 (34)	92.5 (8)
C_{3A}-M_3-M_1	95.6 (5)	94.7 (17)	95.9 (6)
C_{3A}-M_3-M_2	137.3 (5)	138.2 (19)	137.7 (5)
C_{3A}-M_3-S	84.4 (5)	85.1 (17)	84.9 (6)
C_{3B}-M_3-M_1	150.5 (5)	153.2 (22)	151.1 (6)
C_{3B}-M_3-M_2	96.9 (5)	100.6 (22)	97.7 (6)
C_{3B}-M_3-S	99.4 (5)	101.1 (23)	100.1 (6)
C_{3B}-M_3-C_{3A}	88.5 (7)	86.7 (27)	88.1 (8)
C_{3C}-M_3-M_1	118.6 (5)	119.7 (22)	118.2 (6)
C_{3C}-M_3-M_2	133.1 (5)	133.7 (23)	132.9 (6)
C_{3C}-M_3-S	167.7 (5)	168.6 (22)	167.4 (6)
C_{3C}-M_3-C_{3A}	88.9 (7)	87.4 (29)	88.6 (8)
C_{3C}-M_3-C_{3B}	90.6 (7)	87.1 (31)	90.4 (8)
C_{3D}-M_3-M_1	92.7 (4)	91.8 (17)	92.9 (5)
C_{3D}-M_3-M_2	56.5 (4)	55.4 (17)	56.9 (5)
C_{3D}-M_3-S	109.4 (5)	108.5 (18)	109.7 (5)
C_{3D}-M_3-C_{3A}	166.2 (6)	166.2 (26)	165.4 (7)
C_{3D}-M_3-C_{3B}	89.7 (6)	92.9 (28)	89.9 (7)
C_{3D}-M_3-C_{3C}	77.5 (7)	78.8 (27)	77.0 (8)
M_1-S-M_2	76.2 (1	76.5 (7)	76.2 (1)
M_1-S-M_3	76.1 (1)	75.9 (6)	76.0 (1)
M_2-S-M_3	74.6 (1)	74.7 (6)	74.5 (1)

The fourth metal atom attaches itself to the sulfur atom but does not form any metal–metal bonds to the other metal centers of the cluster. The synthesis and molecular structure of $[Cr_4(CO)_{17}S][PPN]_2$ has been previously reported by Hoefler et al.[16] Three metal atoms and the sulfur atom form the tetrahedral core of the cluster. Twelve carbonyl groups coordinate to the three metal atoms, fulfilling their electronic requirements. The remaining metal center bonds to the sulfur atom as a $M(CO)_5$ unit. The sulfido ligand is believed to play an integral role in the condensation of small clusters to form cluster species containing six and nine metal atoms.[17] If this methodology is extended, the controlled synthesis of small metal crystallites may be possible.

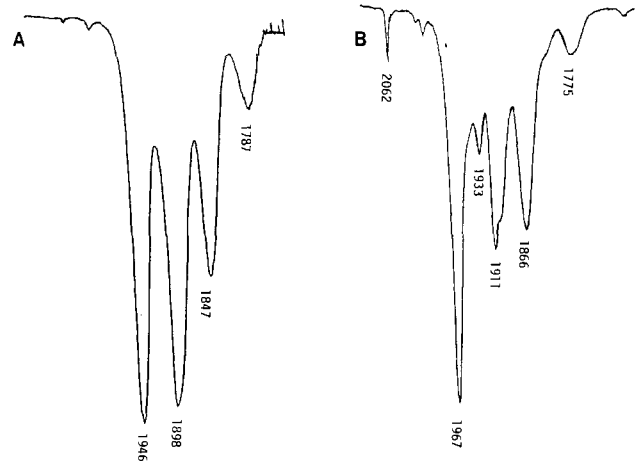

Figure 1. Infrared spectra in the ν_{CO} region of (A) $[(\mu_2\text{-}CO)_3(CO)_9Cr_3(\mu_3\text{-}S)][PPN]_2$ and (B) $[(\mu_2\text{-}CO)_3(CO)_9Cr_3(\mu_4\text{-}S)Cr(CO)_5][PPN]_2$ in THF solution.

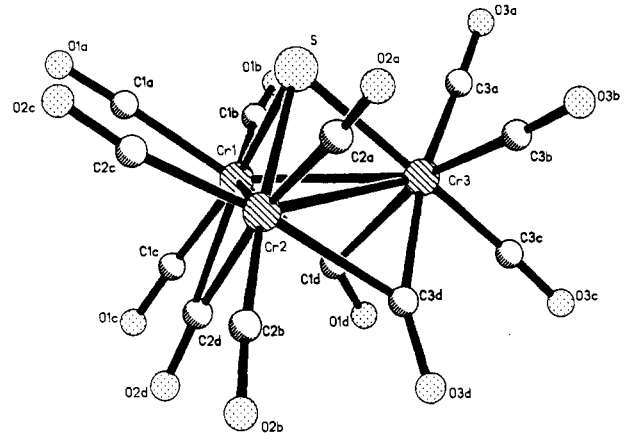

Figure 2. Molecular structure and labeling scheme for the $[Cr_3(CO)_{12}S]^{2-}$ anion.

Formation of the tetramer species can be conveniently monitored by infrared spectroscopy (Figure 1). As the fourth metal atom is coordinated to the sulfur atom the carbonyl bands of the $M_3(CO)_{12}S$ unit are shifted to higher wavenumbers (Table VII). This is consistent with the new metal center withdrawing some electron density away from the M_3S unit. The pattern observed in the infrared spectrum is not just the sum of the $[M_3(CO)_{12}S]^{2-}$ and $M(CO)_5$ moieties, suggesting that the carbonyls of the $M(CO)_5$ unit are coupled to those contained in the $M_3(CO)_{12}$ fragment.

Identical patterns in the infrared and ^{13}C NMR spectra indicate that all of the trinuclear sulfur-capped clusters presented in this paper are isostructural. The infrared stretching frequencies of the $[M_3(CO)_{12}S][PPN]_2$ clusters are listed in Table VII. From the observed pattern, it is clear that the clusters possess a high degree of symmetry. The weak broad band at 1800 cm^{-1} is indicative of unsymmetric or semibridging carbonyl groups.[18]

In order to fully characterize this cluster system we have carried out an X-ray diffraction analysis on three $[M_3(CO)_{12}S][PPN]_2$ clusters. The molecular arrangement and numbering scheme of

(16) Hoefler, M.; Tebbe, K.-F.; Veit, H.; Weiler, N. E. *J. Am. Chem. Soc.* **1983**, *105*, 6338.

(17) Adams, R. D.; Dawoodi, Z.; Foust, D. F.; Segmuller, B. E. *J. Am. Chem. Soc.* **1983**, *105*, 831.

(18) Colton, R.; McCormick, M. J. *Coord. Chem. Rev.* **1980**, *31*, 1.

Table VII. Infrared Stretching Frequencies of Group 6 Sulfido Complexes

complex[a]	ν_{CO}, cm^{-1}							
$Cr(CO)_5SH^-$	2040 (w)	1909 (vs)	1842 (m)					
$Mo(CO)_5SH^-$	2052 (w)	1967 (sh)	1915 (vs)	1846 (m)				
$W(CO)_5SH^-$	2051 (w)	1911 (vs)	1846 (m)					
$Cr_2(CO)_{10}SH^-$	2062 (vw)	2044 (w)	1967 (sh)	1935 (vs)	1909 (m)	1874 (m)		
$Mo_2(CO)_{10}SH^-$	2068 (vw)	2056 (w)	1961 (sh)	1940 (vs)	1871 (m)			
$W_2(CO)_{10}SH^-$	2068 (vw)	2056 (w)	1966 (sh)	1934 (vs)	1906 (m)	1879 (m)		
$CrMo(CO)_{10}SH^-$	2057 (vw)	2049 (w)	1968 (sh)	1939 (vs)	1913 (m)	1873 (m)		
$CrW(CO)_{10}SH^-$	2065 (vw)	2055 (w)	2049 (w)	1967 (sh)	1936 (vs)	1909 (m)	1872 (m)	
$WMo(CO)_{10}SH^-$	2056 (w)	1967 (sh)	1937 (vs)	1911 (m)	1870 (m)			
$Cr_3(CO)_{12}S^{2-}$	2008 (w)	1946 (vs)	1898 (s)	1847 (m)	1787 (w, br)			
$Mo_3(CO)_{12}S^{2-}$	2017 (w)	1968 (vs)	1941 (m)	1906 (vs)	1897 (sh)	1845 (m)	1808 (nw, br)	
$W_3(CO)_{12}S^{2-}$	2016 (w)	1966 (s)	1905 (vs)	1846 (m)	1799 (w, br)			
$Cr_2W(CO)_{12}S^{2-}$	2014 (w)	1957 (s)	1901 (vs)	1846 (m)	1798 (w, br)			
$Mo_2Cr(CO)_{12}S^{2-}$	2019 (w)	1965 (sh)	1948 (s)	1899 (vs)	1846 (m)	1791 (w, br)		
$Mo_2W(CO)_{12}S^{2-}$	2039 (w)	2019 (w)	1970 (s)	1908 (s)	1900 (s)	1847 (m)	1803 (w, br)	
$CrMoW(CO)_{12}S^{2-}$	2040 (w)	1967 (s)	1907 (vs)	1900 (sh)	1848 (m)	1796 (w, br)		
$Cr_4(CO)_{17}S^{2-}$	2062 (w)	2020 (vw)	1967 (vs)	1933 (w)	1911 (m)	1904 (sh)	1866 (m)	1795 (w, br)
$Mo_4(CO)_{17}S^{2-}$	2068 (w)	2057 (w)	1981 (vs)	1939 (vs)	1918 (m)	1907 (sh)	1862 (m)	1815 (w, br)
$Cr_3W(CO)_{17}S^{2-}$	2062 (w)	2042 (w)	1967 (vs)	1936 (vs)	1911 (m)	1903 (sh)	1971 (m)	1792 (w, br)

[a] The spectra were recorded in THF by using the PPN^+ salt of the complex.

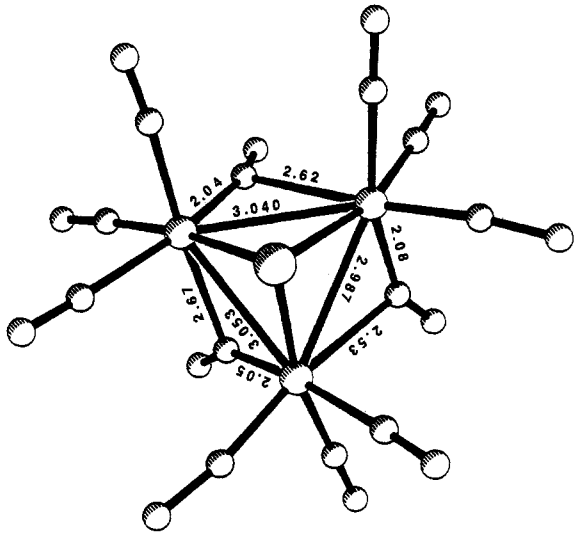

Figure 3. Bond lengths (Å) about the trinuclear molybdenum cluster, indicating the semibridging CO ligands.

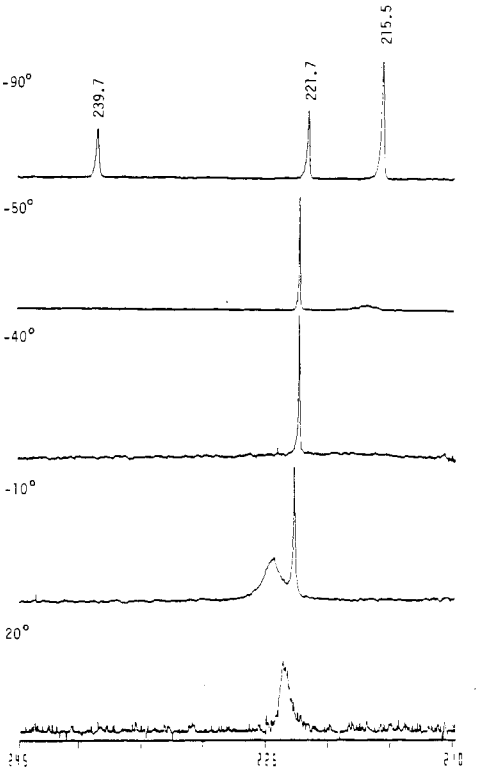

Figure 4. Temperature-dependent ^{13}C NMR spectra of $[Mo_3(CO)_{12}S][PPN]_2$.

the anion is illustrated in Figure 2. The core of the cluster consists of a tetrahedral M_3S unit. This μ_3-S arrangement is common in sulfido clusters.[19] The 12 carbonyl ligands of the cluster fulfill the electron requirement of the metal atoms and are located in three chemically distinct positions. Three of the carbonyl groups adopt a bridging configuration between adjacent metal centers. These μ_2-CO ligands lie below the plane formed by the metal atoms. Three carbonyl ligands take up a position trans to the sulfur atom. These CO groups are also located below the plane of the metal atoms. The remaining six CO groups are situated above the metal atom plane and are cis to the sulfur ligand. If one neglects the rather long M–M bonds, each metal atom possesses a distorted octahedral ligand arrangement.

Tables V and VI compare the bond distances and bond angles in the Cr_3, Mo_3 and Mo_2W clusters. Since all of the clusters are isostructural, we will focus our attention on the Mo_3 cluster and point out any differences in the observed trend. The triangle formed by the three Mo atoms consist of two long (3.053 (2), 3.040 (2) Å) M–M bonds and one short (2.987 (2) Å) M–M bond. This difference of 0.060 Å causes a slight asymmetry to exist in the cluster system. This asymmetry is also reflected in the M–S bonds, where one M–S bond distance is 0.014 (4) Å shorter than the other two. This shortening is only slightly greater than 3σ and may be caused by crystal packing forces. However a similar shortening is seen for the Cr_3 cluster and to lesser extent in the Mo_2W cluster.

The carbonyl groups located trans to the electron rich sulfur atom (C_{1B}, C_{2B}, C_{3B}) contain M–CO bonds that are considerably shorter then the remaining terminal M–CO bonds. This feature is analogous to the shortening seen in simple organometallic compounds.[20] The bond distance reflects an increase in the

(19) Some of the many references in this area include the following: (a) Marko, L.; Madach, T.; Vahrenkamp, H. *J. Organomet. Chem.* **1980**, *190*, C67. (b) Vahrenkamp, H. *Adv. Organomet. Chem.* **1983**, *22*, 169. (c) Adams, R. D.; Horvath, I. T.; Kim, H.-S. *Organometallics* **1984**, *3*, 548. (d) Adams, R. D.; Horvath, I. T.; Seqmuller, B. E.; Yang, L. *Organometallics* **1983**, *2*, 144. (e) Adams, R. D.; Horvath, I. T.; Mathur, P. *J. Am. Chem. Soc.* **1983**, *105*, 1983. (f) Adams, R. D.; Yang, L. *J. Am. Chem. Soc.* **1983**, *105*, 235. (g) Adams, R. D.; Hor, T. S. A.; Mathur, P. *Organometallics* **1984**, *3*, 634. (h) Adams, R. D.; Hor, T. S. A. *Inorg. Chem.* **1984**, *23*, 4723.

Scheme I

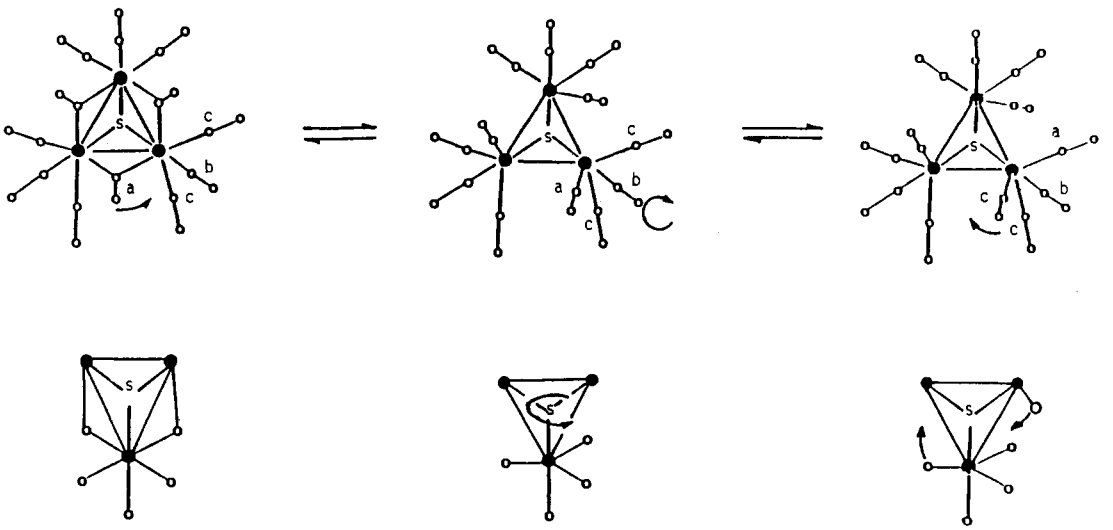

"π-back-bonding" from the Mo center to the antibonding orbital of the carbon monoxide group.

The length of the metal–metal bonds causes the μ_2-CO ligands to adopt a semibridging arrangement. Hence each bridging carbonyl possesses one short and one long M–CO bond (Figure 3). The semibridging arrangement adopted by this cluster system imparts a chirality into the system. The fluxionality of the carbonyl groups equilibrates these different isomers in solution (vide infra).

The low-temperature ^{13}C NMR spectra contain three resonances in the carbonyl region (Figure 4, see also the figure in ref 10 for the Cr analogue). These signals indicate that the CO ligands in the $[M_3(CO)_{12}S][PPN]_2$ clusters adopt three chemically distinct environments, namely, one set of bridging CO groups and two sets of terminal CO groups. Furthermore, from the integrated intensity it is shown that these ligand positions are occupied in a 3:3:6 ratio, respectively. This pattern is only consistent with the solid-state structure if it is assumed that either the chemical shift differences in the cis terminal CO ligands (c) are small or their equivalence in the NMR is due to an averaging process that interchanges the enantiomers as illustrated in eq 2.

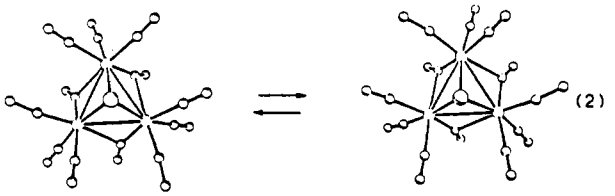

(2)

The labeling designation shown in Scheme I will be used to interpret the fluxionality observed in the ^{13}C NMR spectra. The most downfield resonance is assigned to the three bridging or semibridging carbonyl groups (a). The middle resonance can be assigned to the three CO groups trans to the sulfur atom (b). The remaining six CO ligands give rise to the most upfield signal (c). As anticipated, the resonances for the three terminal CO ligands located trans to the sulfur atom are located downfield from the resonances of the six cis CO groups. This is consistent with what is noted in the monomeric $M(CO)_5SH^-$ species[11] and contrasts with the assignment made by Hoefler et al., where the trans CO groups were assigned to the upfield resonance.[16]

Table VIII. Variable-Temperature ^{13}C NMR Frequencies of the $[M_3(CO)_{12}S][PPN]_2$ Clusters

cluster	temp, °C	resonance, ppm
$[Cr_3(CO)_{12}S][PPN]_2$	−100	254.0 (a), 236.1 (b), 229.7 (c)
	−80	243.2 (a), 236.1 (b), 229.9 (c)
	−60	235.8 (b), 230.8 (c)
	−40	237.0 (a,b), 235.9 (b)
	−20	237.8 (a,b), 235.9 (b)
	20	237.4 (a,b,c)
	50	237.3 (a,b,c)
$[Mo_3(CO)_{12}S][PPN]_2$	−100	239.7 (a), 221.7 (b), 215.5 (c)
	−90	238.5 (a), 221.7 (b), 215.8 (c)
	−50	222.4 (b), 217.1 (c)
	−40	222.5 (b)
	−10	224.5 (a,c), 222.9 (b)
	20	223.7 (a,b,c)
$[W_3(CO)_{12}S][PPN]_2$[a]	−90	224.7 (a), 214.0 (b), 204.5 (c)
	−40	225.8 (a), 214.9 (b), 205.7 (c)
	−10	215.2 (b)
	25	213.6 (b), 211.2 (a,c)

[a] The carbonyl resonances are coupled to the tungsten atoms: J_a = 26.3 Hz, J_b = 76.3 Hz, and J_c = 81.3 Hz.

Scheme II

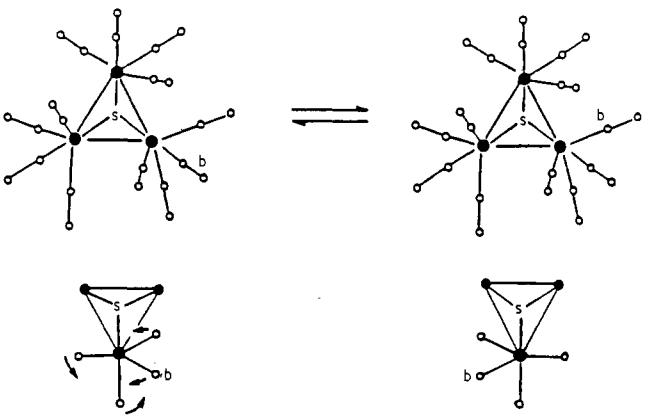

As the solution is warmed up, two distinct intramolecular carbonyl migration processes can be observed. The lower energy process involves an equilibration of the bridging and cis carbonyl ligands. This can be seen by the gradual broadening of the a and c resonances as the temperature is raised. These resonances dissappear from the spectrum, and a new resonance located at their statistical mean grows in. The higher energy process equilibrates the trans CO groups (b) with the a and c sites. The chemical shift values observed in the ^{13}C NMR spectra as a function of temperature are presented in Table VIII.

(20) (a) Darensbourg, D. J.; Rokicki, A. *Organometallics* **1982**, *1*, 1685. (b) Cotton, F. A.; Darensbourg, D. J.; Kolthammer, B. W. S. *J. Am. Chem. Soc.* **1981**, *103*, 398. (c) Cotton, F. A.; Darensbourg, D. J.; Kolthammer, B. W. S.; Kudaroski, R. *Inorg. Chem.* **1982**, *21*, 1656. (d) Darensbourg, D. J.; Walker, N.; Darensbourg, M. Y. *J. Am. Chem. Soc.* **1980**, *102*, 1213. (e) Darensbourg, D. J.; Walker, N.; Darensbourg, M. Y. *Inorg. Chem.* **1981**, *20*, 1918. (f) Darensbourg, D. J.; Pala, M.; Waller, J. *Organometallics* **1983**, *2*, 1285.

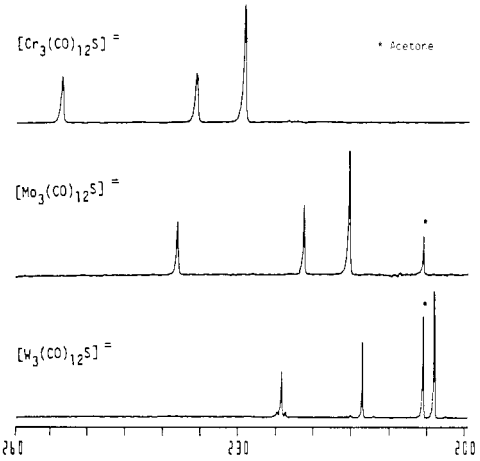

Figure 5. Low-temperature ^{13}C NMR spectra of the $[M_3(CO)_{12}S][PPN]_2$ clusters.

The facile carbonyl migration occuring in these clusters is best described by Schemes I and II. The lower energy equilibrium cannot be explained by a simple merry-go-round process, since the nine carbonyl ligands involved (sites a and c) are not coplanar.[21] Instead, the process can be rationalized by invoking a bridging to terminal motion of the carbonyl ligands, followed by rotation about the metal–sulfur bond (Scheme I). Converting the bridging CO ligands into terminal groups causes the local metal geometry to change from octahedral to trigonal bipyramidal. This motion leaves the a carbonyls located below the plane of the metal atoms, while the c carbonyls are positioned above the metal atom plane. Thus, rotation about the metal–sulfur bond is required to equilibrate the two sites. The higher energy process could proceed through the same trigonal-bipyramidal intermediate generated in the lower energy process. Once this intermediate is formed a pseudorotation would cause an equilibrium of all twelve CO groups. The schematic details of this motion are depicted in Scheme II.

Careful inspection of Table VIII reveals that the carbonyl migration process takes place at higher temperatures as one proceeds down the periodic table. That is, the rate of carbonyl scrambling decreases in the following order: $Cr_3 > Mo_3 > W_3$. Since the third-row tungsten atom forms stronger M–CO bonds than either the first or second row elements, it is anticipated that migration of carbonyl ligands about the W_3 centers will be the least facile. At −100 °C the ^{13}C resonances due to carbonyl ligands a and c of the Cr_3 and Mo_3 clusters are separated by 1218 and 1142 Hz, respectively. At −40 °C the a and c sites in the Cr_3 cluster are rapidly exchanging, and a resonance at 237.0 ppm appears in the spectrum. On the other hand, the Mo_3 cluster requires a temperature of −10 °C before this intramolecular CO exchange is rapid. Since the separation of the a and c resonances in the Cr_3 cluster is slightly greater than that of the Mo_3 cluster, the observed fluxionality differences are real.

As one proceeds down the periodic table from chromium to tungsten, the carbonyl resonances gradually shift upfield (Figure 5). This property provides us with a sensitive probe for determining whether or not the cluster's integrity remains intact during a reaction. For example, the intermolecular carbon monoxide exchange reaction between $[Cr_3(CO)_{12}S][PPN]_2$ and $[Mo_3(^{13}CO)_{12}S][PPN]_2$ can be monitored by ^{13}C NMR spectroscopy. If the clusters exchange CO ligands without homolysis of the metal–metal bonds, then the labeled ^{13}C ligand should be evenly distributed between the two clusters as shown in eq 3. However

$$[Cr_3(CO)_{12}S]^{2-} + [Mo_3(^{13}CO)_{12}S]^{2-} \rightleftarrows [Cr_3(^*CO)_{12}S]^{2-} + [Mo_3(^*CO)_{12}S]^{2-} \quad (3)$$

if the scrambling process occurs via cluster fragmentation, one would expect to see the mixed metal clusters as illustrated in eq 4. The spectrum taken immediately after the above two clusters

$$[Cr_3(CO)_{12}S]^{2-} + [Mo_3(^{13}CO)_{12}S]^{2-} \not\rightarrow [Cr_2Mo(^*CO)_{12}S]^{2-} + [Mo_2Cr(^*CO)_{12}S]^{2-} \quad (4)$$

$$^*CO = {}^{13}CO/{}^{12}CO$$

were mixed shows strong resonances assigned to the enriched Mo_3 cluster. After the solution was allowed to stand at room temperature for 2 h, resonances assigned to the Cr_3 cluster grew in. Signals assigned to the mixed-metal clusters $[Cr_2Mo(CO)_{12}S][PPN]_2$ or $[Mo_2Cr(CO)_{12}S][PPN]_2$ were not observed. This indicates that these clusters do not fragment under these conditions.

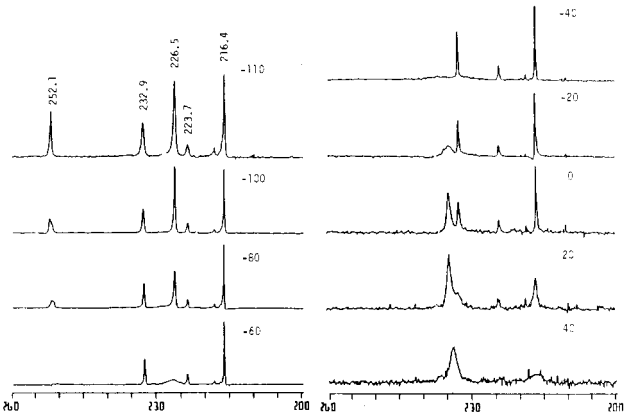

Figure 6. Temperature-dependent ^{13}C NMR spectra of $[Cr_4(CO)_{17}S][PPN]_2$.

The tetranuclear derivatives display the same type of facile carbonyl scrambling observed in the trinuclear clusters. It was necessary to observe the ^{13}C NMR spectrum of the tetrachromium cluster at −110 °C to completely freeze out the ligand migration process. This is a slightly lower temperature than that needed for the $[Cr_3(CO)_{12}S][PPN]_2$ cluster. This difference is probably caused by the decrease in the donating ability of the S ligand to the Cr_3 unit as a result of the appended $M(CO)_5$ ligand.

The trinuclear portion of $[(\mu_2\text{-}CO)_3(CO)_9Cr_3(\mu_4\text{-}S)Cr(CO)_5]^{2-}$ exhibits a ^{13}C NMR spectrum with resonances corresponding to the a, b, and c sites located at 252.1, 232.9, and 226.5 ppm, respectively. These signals are shifted upfield from those observed for the trinuclear cluster, consistent with the appended $Cr(CO)_5$ unit withdrawing some of the negative charge associated with the trinuclear cluster. The pentacarbonyl portion of the molecule displays two resonances in a 1:4 ratio at 223.7 (CO_{trans}) and 216.4 ppm (CO_{cis}), respectively.

The temperature dependence of the ^{13}C NMR spectrum of $[Cr_4(CO)_{17}S]PPN_2$ is shown in Figure 6. The resonances for the a and c carbonyls broaden in the −80 to −60 °C region. At −40 °C these signals disappear from the spectrum but reappear at their statistical mean as the temperature is raised to −20 °C. The b carbonyls become involved in the scrambling process at temperatures greater than 0 °C. The appended $Cr(CO)_5$ unit enters the exchange process at temperatures greater than 10 °C.

The facile nature of the carbon monoxide migration occuring in this cluster is demonstrated by eq 5. When $[Cr_3(CO)_{12}S]^{2-}$

$$[(\mu_2\text{-}CO)_3(CO)_9Cr_3(\mu_3\text{-}S)]^{2-} + Cr(^{13}CO)_5\cdot THF \rightarrow [(\mu_2\text{-}^*CO)_3(^*CO)_9Cr_3(\mu_4\text{-}S)Cr(^*CO)_5]^{2-} \quad (5)$$

$$^*CO = {}^{12}CO/{}^{13}CO$$

is reacted with ^{13}C enriched $Cr(CO)_5$·THF, the labeled ^{13}CO ligands end up being statistically distributed throughout the cluster. The method in which these labeled ligands are distributed throughout the cluster could initially involve metal atom migration. That is, the appended $Cr(CO)_5$ unit could become part of the Cr_3 triangle by the redistribution of the carbon monoxide ligands. This requires one of the chromium atoms of the $(Cr_3(CO)_{12})$ portion

(21) Band, E.; Muetterties, E. L. *Chem. Rev.* **1978**, *78*, 639.

to migrate to the apical position and become the pentacarbonyl portion of the molecule. Close examination of the X-ray structure of $[Cr_4(CO)_{17}S]^{2-}$ reveals that the appended $Cr(CO)_5$ unit is bent down toward the chromium triangle. Hence, the above mentioned motion is not unrealistic.

Further evidence for this metal atom migration is provided by the $[Cr_3W(CO)_{17}S]^{2-}$ cluster. When $[Cr_3(CO)_{12}S]^{2-}$ is reacted with $W(CO)_5$·THF, the infrared spectrum displays a pattern identical with that of $[Cr_4(CO)_{17}S]^{2-}$. However a complex pattern emerges in the ^{13}C NMR spectra. An identical pattern is obtained when $[Cr_2W(CO)_{12}S]^{2-}$ is reacted with $Cr(CO)_5$·THF. This suggest the presence of two isomers, $[(\mu_2\text{-}CO)_3(CO)_9Cr_3(\mu_4\text{-}S)W(CO)_5]^{2-}$ and $[(\mu_2\text{-}CO)_3(CO)_9Cr_2W(\mu_4\text{-}S)Cr(CO)_5]^{2-}$ (eq 6).

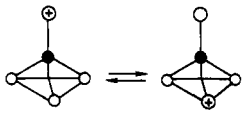

(6)

Comparing the intensities of the resonance assigned to the $Cr(CO)_5$ unit (215.9 ppm) to that assigned to the $W(CO)_5$ unit (198.1 ppm) reveals that the two isomers are present in a 1:3 ratio. This ratio represents the statistical distribution of the metal atoms about the cluster.

Conclusions

We have exploited the coordinating ability of a naked sulfur atom and utilized it as a template to construct a variety of group 6 cluster compounds. By careful control of the reaction conditions, selective aggregation of metal fragments can be achieved. This provides us with the synthetic methodology to construct mixed-metal clusters, such as the chiral cluster $[CrMoW(CO)_{12}S][PPN]_2$. The technique of metal atom aggregation should provide a general route to the synthesis of discrete transition-metal clusters containing a chiral metal framework. These new sulfur-capped cluster systems display very facile carbonyl migration processes. Variable-temperature NMR studies indicate that these CO scrambling processes cannot be explained by existing migration mechanisms; alternative fluxional processes are proposed.

Acknowledgment. The financial support of the Robert A. Welch Foundation is greatly appreciated.

Registry No. $[Cu_3(CO)_{12}S][PPN]_2$, 112680-67-8; $[Mo_3(CO)_{12}S][PPN]_2$, 112680-70-3; $[W_3(CO)_{12}S][PPN]_2$, 112680-72-5; $[Cr_2W(CO)_{12}S][PPN]_2$, 112680-74-7; $[Mo_2W(CO)_{12}S][PPN]_2$, 112680-77-0; $[CrMoW(CO)_{12}S][PPN]_2$, 112680-79-2; $Cr(CO)_6$, 13007-92-6; $Cr(CO)_5$THF, 15038-41-2; $Mo(CO)_6$, 13939-06-5; $Mo(CO)_5$THF, 53248-43-4; $W(CO)_6$, 14040-11-0; $W(CO)_5$THF, 36477-75-5; $[Cr(CO)_5SH][PPN]$, 71688-47-6; $[Mo(CO)_5SH][PPN]$, 71688-49-8; $[W(CO)_5SH][PPN]$, 71771-28-3; $[Cr_2(CO)_{10}SH][PPN]$, 77310-17-9; $[Mo_2(CO)_{10}SH][PPN]$, 112680-80-5; $[W_2(CO)_{10}SH][PPN]$, 112680-81-6; $[CrMo(CO)_{10}SH][PPN]$, 112680-83-8; $[CrW(CO)_{10}SH][PPN]$, 112680-85-0; $[WMo(CO)_{10}SH][PPN]$, 112680-87-2; $[Mo_2Cr(CO)_{12}S][PPN]_2$, 112680-89-4; $[Cr_4(CO)_{17}S][PPN]_2$, 87050-04-2; $[Mo_4(CO)_{17}S][PPN]_2$, 112680-93-0; $[(\mu_2\text{-}CO)_3(CO)_9Cr_2W(\mu_4\text{-}S)Cr(CO)_5][PPN]_2$, 112680-95-2; $[(\mu_2\text{-}CO)_3(CO)_9Cr_3(\mu_4\text{-}S)W(CO)_5][PPN]_2$, 112680-91-8.

Supplementary Material Available: Complete listings of atomic coordinates and temperature factors for both cation and anion and anisotropic temperature factors and low-temperature ^{13}C NMR spectra of an equimolar mixture of $[Cr_3(CO)_{12}S][PPN]_2$ and $[Mo_3(^{13}CO)_{12}S][PPN]_2$ and ^{13}C NMR spectra of $[Cr_3W(CO)_{17}S][PPN]_2$ (14 pages); tables of observed and calculated structure factors (82 pages). Ordering information is given on any current masthead page.

Contribution from the Dipartimento di Chimica dell'Università di Venezia, 30123 Venice, Italy, and Istituto di Chimica Generale, Centro Strutturistica CNR, Università di Parma, 43100 Parma, Italy

Bis(aryldiazene)- and Related Mono(aryldiazenido)ruthenium Complexes: Preparation, Characterization, and Reactivity. Crystal Structure of $[Ru(4\text{-}CH_3C_6H_4N{=}NH)_2\{P(OEt)_3\}_4](PF_6)_2$

Gabriele Albertin,[1a] Stefano Antoniutti,[1a] Giancarlo Pelizzi,[1b] Francesca Vitali,[1b] and Emilio Bordignon*[1a]

Received April 17, 1987

Complexes $[Ru(ArN{=}NH)_2L_4](BPh_4)_2$ (**1**) and $[RuH(ArN{=}NH)L_4]BPh_4$ (**2**) [L = $P(OEt)_3$; Ar = C_6H_5, 4-$CH_3C_6H_4$, 4-$CH_3OC_6H_4$, 4-FC_6H_4, 2,6-$Cl_2C_6H_3$, 2,3-$Cl_2C_6H_3$] were synthesized by allowing the hydride $RuH_2[P(OEt)_3]_4$ to react with aryldiazonium cations; their characterization by ^1H and $^{31}P\{^1H\}$ NMR (with ^{15}N isotopic substitution) is reported. Atom connectivity in the cation $[Ru(4\text{-}CH_3C_6H_4N{=}NH)_2\{P(OEt)_3\}_4]^{2+}$ is determined by a low-precision X-ray structure determination of its PF_6^- salt. Crystals are monoclinic, space group $P2_1/n$, with unit cell dimensions a = 23.319 (3) Å, b = 22.328 (3) Å, c = 11.513 (2) Å, β = 91.93 (1)°, and Z = 4. The structure was solved by heavy-atom methods and refined by least squares to an R index of 0.0969. The geometry around the ruthenium atom is essentially octahedral with the two diazene ligands in cis positions. The reaction of the bis(aryldiazene) derivatives **1** with NEt_3 leads to new pentacoordinate aryldiazenido $[Ru(ArN_2)\{P(OEt)_3\}_4]^+$ (**3**; Ar = C_6H_5, 4-$CH_3C_6H_4$, 4-FC_6H_4) complexes. Protonation reactions with HBF_4 and CF_3COOH of these aryldiazenido compounds **3** afforded $[Ru(ArN{=}NH)\{P(OEt)_3\}_4](BPh_4)_2$ and $[Ru(CF_3COO)(ArN{=}NH)\{P(OEt)_3\}_4]BPh_4$ (Ar = 4-$CH_3C_6H_4$) derivatives, respectively. Lastly, a new series of ruthenium(II) complexes of the types *trans*-$[Ru(ArN{=}NH)(CO)L_4]^{2+}$, *cis*- and *trans*-$[RuCl(CO)L_4]^+$, $[Ru(ArN{=}NH)L_5]^{2+}$, $[RuCl(4\text{-}CH_3C_6H_4NC)_2L_3]^+$, $[Ru(4\text{-}CH_3C_6H_4NC)_3L_3]^{2+}$, and *cis*-$[RuCl(4\text{-}CH_3C_6H_4N{=}NH)L_4]^+$ (Ar = 4-$CH_3C_6H_4$) were prepared by ligand-substitution reaction of both **1** and **2** derivatives. Their characterization by infrared and ^1H and $^{31}P\{^1H\}$ NMR spectra is also reported.

Introduction

We recently reported[2] the synthesis of the first example of a bis(diazene) complex, $[Fe(ArN{=}NH)_2\{P(OEt)_3\}_4]^{2+}$, obtained by the "apparent" insertion of two aryldiazonium groups into the Fe–H bond of the FeH_2L_4 hydride. Since polyhydrides of Ru, Os, Rh, Ir, W, and Re are known to react with diazonium salt to give mono(diazene) or mono(hydrazido) complexes in any case,[3] we extended this reaction to other dihydrides in order to test whether the formation of bis(diazene) complexes is a general

(1) (a) Università di Venezia. (b) Università di Parma.
(2) Albertin, G.; Antoniutti, S.; Pelizzi, G.; Vitali, F.; Bordignon, E. *J. Am. Chem. Soc.* **1986**, *108*, 6627.
(3) (a) Laing, K. R.; Robinson, S. D.; Uttley, M. F. *J. Chem. Soc., Dalton Trans.* **1973**, 2713. (b) Toniolo, L.; Eisenberg, R. *J. Chem. Soc. D* **1971**, 455. (c) Carroll, J. A.; Sutton, D.; Cowie, M.; Gauthier, M. D. *J. Chem. Soc., Chem. Commun.* **1979**, 1058. (d) Carroll, J. A.; Sutton, D. *Inorg. Chem.* **1980**, *19*, 3137. (e) Cowie, M.; Gauthier, M. D. *Inorg. Chem.* **1980**, *19*, 3142. (f) Einstein, F. W. B.; Jones, T.; Hanlan, A. J. C.; Sutton, D. *Inorg. Chem.* **1982**, *21*, 2585.

0020-1669/88/1327-0829$01.50/0